New coloured coatings to enhance silica sand absorbance for direct particle solar receiver applications

A. Gimeno-Furio[1], L. Hernandez[1*], R. Martinez-Cuenca[1], R. Mondragón[1], A. Vela[1] L. Cabedo[2], C. Barreneche[3,4], M. Iacob[5]

[1] Department of Mechanical Engineering and Construction, Universitat Jaume I, Castelló de la Plana, Spain

[2] Polymers and Advanced Materials Group (PIMA), Universitat Jaume I, Castelló de la Plana, Spain

[3] Department of Materials Science and Physical Chemistry, Universitat de Barcelona, Barcelona, Spain

[4] Birmingham Centre for Energy Storage & School of Chemical Engineering, University of Birmingham, United Kingdom

[5] Petru Poni Institute of Macromolecular Chemistry Iasi, Romania

*Corresponding author: lhernand@emc.uji.es

Abstract

New systems using solid particles for solar energy capturing, heat transfer and thermal energy storage have been proposed and analysed in direct particle solar receivers. In this work, black coloured silica sand was investigated as a possible solid particle for such combined systems. Two different methods based on a carbon coating approach were implemented to black colour the initial material to improve their solar absorption characteristics. The morphology of the raw and coloured sands was analysed by scanning electron microscopy (SEM), particle size characterisation and porosity measurements. The coating of the black-coloured silica sands was evaluated by thermogravimetry. Solar absorption was characterised in a double-beam UV-VIS spectrophotometer combined with an integrating sphere, and with enhancements of approximately 100%, found for both coloured sands. The thermal storage and heat transfer capabilities of the initial and coated sands were measured at different temperatures. Some improvements in the specific heat capacity and reductions in thermal conductivity due to porosity changes were observed.

Key words: Solar energy, nanoparticles, silica sand, absorption, thermal conductivity

1. INTRODUCTION

The increasing demand of energy together with the present scenario of climate change concerns and decreasing available fossil fuel resources have motivated a rapid deployment, development and implementation and improvements of solar thermal receiver technologies. However, additional increases of the efficiency power cycles and reduction of the levelized cost of energy of these systems are being investigated, and Particle Solar Receivers (PSR) have been identified as an interesting option [1].

PSR use solid particles that are heated by concentrated solar radiation and apart to be used as heat transfer media may be used to store energy. In contrast with conventional solar receivers, PSR present some advantages as [2]: wide range of operating temperatures (beyond 600 ºC without corrosion and below 200 ºC without freezing risks as in molten salts), higher power efficiencies due to higher operating temperatures, direct storage of heat transfer media for energy production beyond solar hours, and use of relatively inexpensive and inert working media.

Two main PSD have been developed: direct and indirect. Direct PSD where the radiation is directly absorbed by the material and indirect PSR, in which certain surfaces are used to confine and also heat the particles. Comparative analysis of different configurations of direct PSR (free falling [3], obstructed, centrifugal, fluidized configurations) and indirect PSR (gravity driven flow through enclosures, fluidized flow through tubes, etc) have been recently published (review) [4].

Directly heated particle receivers present the advantage that the media is directly irradiated, eliminating the heat transfer resistance between heated surfaces and particles, reducing exergy losses [5-10]. Several direct PSR projects have been developed at lab or pilot scales since early 1980s [10-15]. Desirable properties of the particles used for direct PSD include high solar absorptance, low cost, wide availability, high heat capacity and durability among others [16]. A variety of particles have been analysed and tested for direct PSD [4], including ceramic particles [17], silicon carbide [18], bauxite [8], alumina [14] and sand [10, 19, 20]. Sand is an inexpensive and abundant media in attractive locations for solar projects; however its solar absorptance is low.

In this work, sand has been black coloured via two different methods in order to improve the absorption capability of the natural sand, one using carbon black (CB) nanoparticles and the other through glucose degradation. The black coating was characterized, including thermal stability at high temperatures. In order to assess the potential of these materials as candidates for direct PSR, different relevant properties of the coloured sand, as solar absorption, thermal conductivity and specific heat capacity were measured and compared to the raw particles.

2. Materials and methods

2.1. Materials

The base material herein studied is silica sand from open-cast mining in Spain. According to the supplier (Silice Gllaranz), sand contains more than 99% SiO_2.

2.2. Coloured sand preparation

Raw sand was black-coloured by two different methods based on a carbon coating approach. Both methods are described and experimentally compared below. All the

mass measurements were taken on an analytical balance during sample synthesis (Kern ABS, ±0.001mg).

The materials used to produce the coating are carbon black (CB) nanoparticles (ELFTEX 570 from Cabot Corporation), anhydrous glucose (Scharlau) and acetone (Guinama). They were all used as received.

2.2.1. Carbon black coating

The first synthesis method to colour sand was based on a carbon black coating. These coloured samples were obtained by suspending 3 grams of carbon black nanoparticles in 240 ml of acetone. The CB nanoparticles were selected by their colour, thermal and chemical stability, and low price. According to the manufacturer, CB nanoparticles are spherical and have an average primary diameter of 10 nm. In order to achieve a good suspension, the mixture was sonicated with an ultrasonic probe (Sonoplus HD2200, Bandelin) for 40 seconds at medium-high power. Then 60 grams of silica sand were added and dispersed in the CB suspension using an ultrasonic probe for 30 seconds at high power. The resulting suspension was poured into a Petri dish and allowed to dry in an oven (Digitronic 2005141, J.P. Selecta, SA) at 100ºC for 15 minutes. In this paper, the coloured samples using this method are denoted as CB sand.

2.2.1. Glucose degradation coating

The second synthesis method to colour sand was based on the generation of a char coating over sand by anaerobic thermal degradation of glucose, where a mixture of 70% sand and 30% glucose in weight was prepared. Distilled water was poured on the vessel to cover the sample and the mixture was stirred for 35 minutes at 55ºC to ensure that glucose was fully dissolved. Water was evaporated by drying thin layers of suspension in an oven at 100ºC. Finally, the dried mixture was placed inside a muffle furnace at 400ºC for 10 minutes at a constant N_2 flow rate to ensure anaerobic atmosphere conditions. This thermal treatment causes cellulose graphitisation and results in a black char coating on sand particles. In this paper, the coloured samples using this method are denoted as Glucose sand.

2.3. Experimental characterisation

Scanning electron microscopy

Scanning electron microscopy (SEM) was performed by JEOL 7001F and JEOL JSM-6510 microscopes equipped with digital image acquisition. Powder samples were observed and the materials' morphology and size were determined. In order to characterise the coatings formed on sand grains, secondary electro images and digital image processing were used.

Particle size

Volume particle size distribution was measured using a laser diffraction analyser (Mastersizer 2000, Malvern). Efficient sample dispersion helps to ensure that the particle size data measured by a laser diffraction analyser are both representative and relevant [21]. Particle size distribution was characterised by volume fraction diameter d_{50}, which

is the value of the particle diameter at 50% in cumulative distribution. According to the manufacturer, the error for the equipment of d_{50} is 3%. Measurements were taken of raw sand and two black-coloured sand samples.

Porosity

Porosity (ε) was calculated with Equation 1:

$$\varepsilon = \frac{\rho_r - \rho_b}{\rho_r} \quad \text{Eq. 1}$$

where ρ_r is the real density of the sample under study (kg m^{-3}) measured with a Helium Pycnometer from Micrometrics, and ρ_b is the bulk density of the same sample (kg m^{-3}) measured by the volume and mass of samples.

Thermogravimetric analysis

A thermogravimetric analysis (TGA) was performed to evaluate the stability of raw sand and also the sand coating in both colouring methods. Tests were run in a thermogravimetric device (Model Simultaneous SDTQ600, TA Instruments) at a synthetic air flow of 50 ml/min. For each sample, around 40 mg were analysed in 100 μL alumina crucibles at a constant heating rate of 10 C/min between 100ºC and 1,000ºC.

Spectrophotometer

The absorption spectrum is one of the most important properties studied herein as it determines the amount of energy absorbed by the pure, CB and glucose sand samples. A UV-Vis-NIR spectrophotometer (CARY 500, Varian Dev) with an integrating sphere was used to measure the absorption spectrum of each sample. This equipment allows spectral measurements to be taken between 250 nm and 2500 nm thanks to two interchangeable lamps [22]. To minimise any effects of undesired reflections and absorptions, the sand samples were placed inside a quartz cuvette with a planar interface (75x25x5 mm).

Figure 1 illustrates the detection geometry of the integrating sphere. Two laser beams are directed to the sphere, one directed to the sample itself and a second acts as a reference. Once the beams enter the sphere, they impact its inner Teflon surface and undergo many internal reflections before being captured by the photodetector (D) at the top of the integrating sphere. Note that the reference beam enters the sphere through a diffusing window (R1) to reduce any losses that might arise from a direct reflection at R2. This beam monitors the laser power changes that occur during the measurement time required for a full wavelength scan. The sample beam enters the integrating sphere through a hole in port S1 and impinges directly onto port S2. In practice, the sample can be placed in either of the two ports, depending on the desired property to be measured. In order to obtain the absorption spectrum, three measurements are needed.

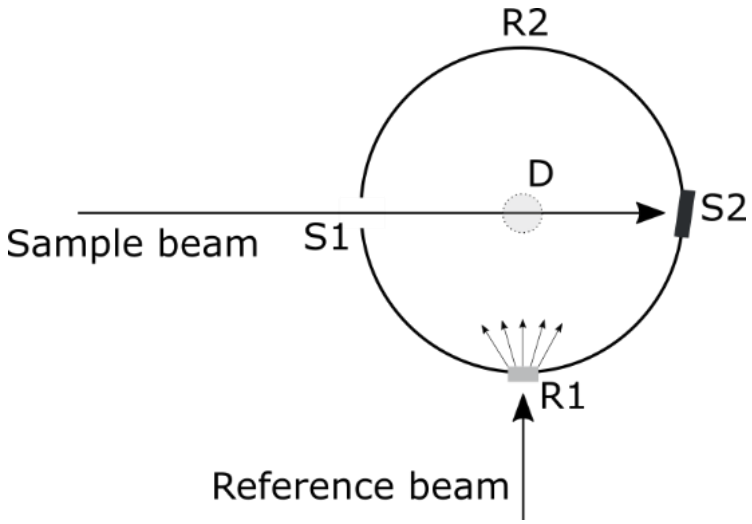

Figure 1. A scheme of the integrating sphere, including the reference and sample beam paths and the measuring port locations (S1 and S2)

The first measurement, named the baseline, is performed by leaving port S1 open and closing port S2 with a Teflon cap. Note that port S2 is tilted about 3° in relation to the normal direction to prevent the direct loss of its specular reflection through port S1. In this configuration, the sample beam enters the integrating sphere, hits the wall and undergoes many reflections before being detected. The intensity at measured the photodetector, I_o, is proportional to the total light power of the sample beam.

For the second measurement, the cuvette with the sample is placed at port S1 and the tilted Teflon cap at port S2. In this configuration, the sample beam first passes through the cuvette with the sample, and the light that emerges on the other side enters the integrating sphere through S1, hits S2 and undergoes many reflections before being detected. The resulting signal intensity, I_{T+FS}, is proportional to the light power that is either directly transmitted through the sample or suffers forward scattering.

In the last measurement, port S1 is left open and the Teflon cap is replaced with the cuvette with the sample at port S2 (the cuvette is also tilted 3° in relation to the normal direction). The resulting signal, I_{R+BS}, is proportional to the sum of the reflected and backward scattered light powers.

Once the three above-mentioned spectrums are measured, absorption spectrum (A) of the sample is obtained through Equation 2:

$$A\ (\%) = \frac{I_0 - I_{T+FS} - I_{R+BS}}{I_0} \cdot 100 \qquad \text{Eq. 2}$$

The measured spectrum range was selected to lie between 400 nm and 1,500 nm with a spectral resolution of 0.5 nm, the 800 to 1,100 nm range was excluded due to the limitations in the experimental set-up caused by the lamps switch and the coupling of both equipment. This range includes visible and part of the near infrared to avoid unreliable spectral ranges of the equipment and comprises 53% of the total solar radiation energy reaching the Earth, including the highest solar radiation level.

Differential scanning calorimetry

Specific heat capacity (*Cp*) was performed to know the validity of the sample as a thermal energy storage material. *Cp* was measured using a Differential Scanning Calorimeter (DSC; Model DSC882e Mettler Toledo). Around 15 mg of each sample were used to run the analyses in 40-μL aluminium crucibles. As the material can undergo oxidation by air, the test was done at a 50 ml/min constant N_2 flow rate between 300ºC and 500ºC with consecutive isothermal segments and the temperature difference between isotherms of 1ºC. Therefore, Cp was measured at 300, 400, and 500ºC. After completing measures, the specific heat capacity was calculated by applying the Areas Methods described by Ferrer et al. [23], which presents relative errors under 4%. The measure was repeated 3 times and the differences found in these three cycles were always less than a 5% relative error. These findings show the reliability of the experimental data.

Conductimeter

The thermal conductivity (k) of all the samples was measured in a KD2 Pro conductimeter (Decagon Devices Inc.). KD2 Pro is a commercial device that measures thermal conductivity by the transient hot wire technique. This technique is based on measuring the temperature/time response of the wire to an electrical pulse. The wire is inserted vertically into the solid sample, which was placed inside a metal tube (70 g). To run the test under high-temperature conditions, the tube was placed in an oven, where temperature was controlled. The test was done at room temperature, 40ºC, 80ºC and 120ºC. Before any testing started, a 1-hour period was needed for the sample to reach the desired temperature. Afterwards, five measurements were taken for all the samples at each temperature.

3. RESULTS AND DISCUSSION

3.1. Silica sand morphology and coating

All the samples under study are shown in Figure 2 to illustrate the difference in colour terms. This is the first time that sand is coloured by this procedure to improve the absorptivity properties and to enhance its direct use as TES materials.

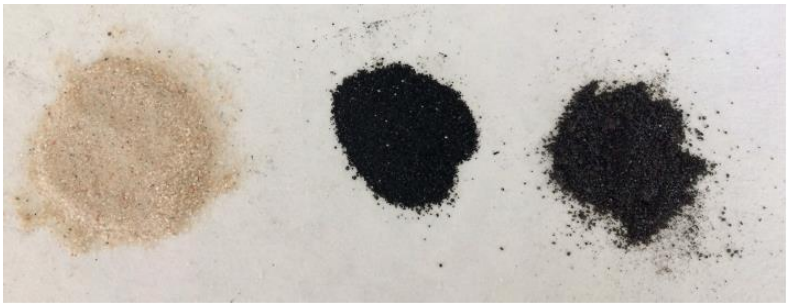

Figure 2. Pure sand, CB sand and Glucose sand (from left to right)

Figure 3 shows the SEM images herein obtained for raw sand and both coated sample types.

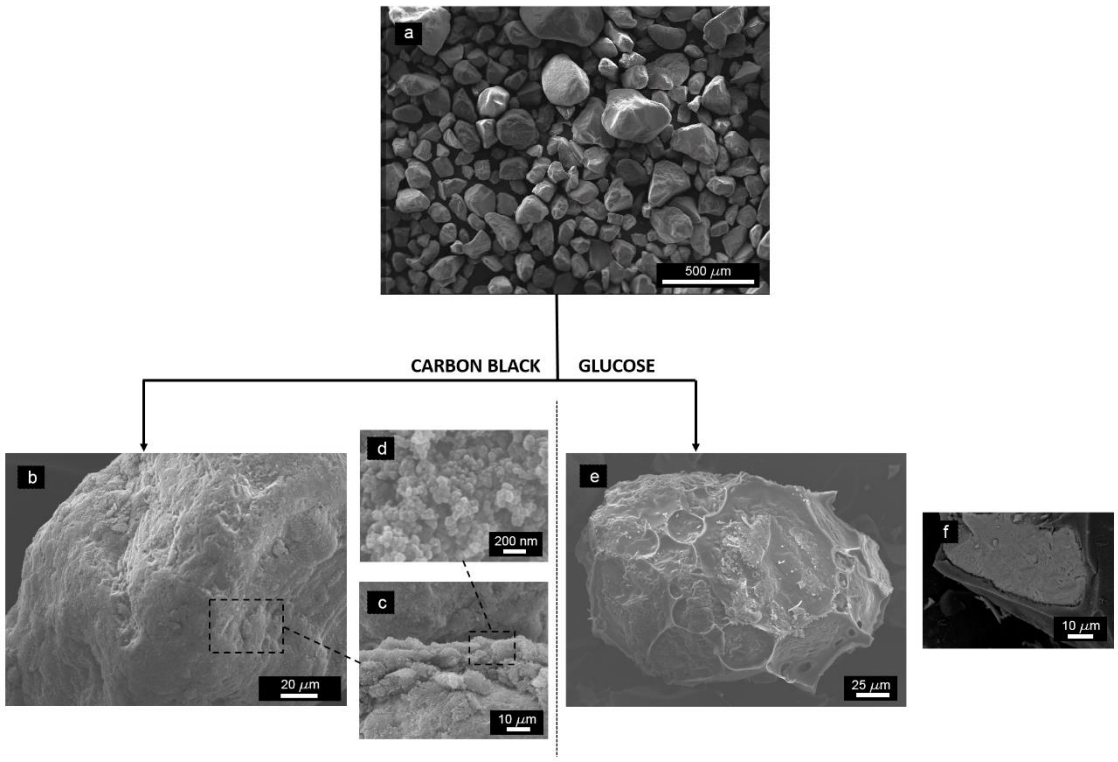

Figure 3. Morphology of sand and carbon-coated sand. (a) SEM micrograph of pristine sand. (b) Carbon black-coated sand granule. (c) Detail of the CB coating. (d) High magnification detail of the carbon black nanoparticles. (e) Glucose-coated sand granule. (f) Detail of the glucose coating.

Figure 3a shows an SEM micrograph of the sand particles as delivered. Sand particles present a spherical geometry with a smooth regular surface given its natural origin. The average d_{50} particle size is 294 µm, as determined by the Mastersizer equipment. Figure 3b presents a CB-coated sand granule, which is fully covered by a homogeneous coating to, thus, present a smooth surface with minor roughness. This uniform coating is formed by myriads of carbon black nanoparticles to form a thick layer. This layer is the result of the agglomeration of CB nanoparticles during the drying process, so that when acetone is fully removed, the graphite nanospheres tend to agglomerate and result in a well-packed layer (see Figure 3d). Nanoparticles are therefore clustered by an electrostatic interaction effect. Figure 3c shows the edge of a broken coating where the carbon black layer morphology is observed. The thickness of the layer falls within the range of tens of microns and the measured average particle size of the CB coated particles is 343 µm.

A single representative sand granule coated by glucose graphitisation is presented in Figure 3e. The granule surface, unlike the CB-coated one, is very irregular, as derived from a heterogeneous char coating. A remarkable increase in surface roughness was observed due to the presence of this particular structure of ridges and valleys that derives from boiling glucose in the graphitisation step. The thickness of the coating can vary considerably from the ridges (up to several tenths of microns), while it can be less than 5 microns in the valley (see Figure 3f). The average particle size for this coating approach is 405 µm.

To analyse the possible impacts of the carbon coating on sand morphology, the porosity of the different samples was evaluated. The porosity of the three sand samples was calculated by real density (ρ_r) and bulk density (ρ_b) using Eq.1. The results are shown in Table 1.

Table 1. Real and bulk densities and porosity values of the three sand samples

	Real density (kg/m^3)	Bulk density (kg/m^3)	Porosity (-)
Sand	2634.9	1615.5	0.387
CB Sand	2581.2	1048.9	0.594
Glucose sand	2595.5	733.3	0.717

The porosity values for the pure sand agree with those found in the bibliography [10, 24], which ranged from 0.312 to 0.417. The results showed that the porosity values increased when sand was coloured. The porosity differences between both coloured sands could be due to the chemistry involved in the way the black coating was linked to sand. Therefore, the CB coating would be bonded more effectively with a smoother surface coating and fewer air cavities inside molecules because porosity was lower than in the glucose sand, where the coating surface presented more roughness.

The amount of graphite present in both the CB-coated and glucose-coated sands was determined by thermogravimetry at an air flow up to 1,000ºC to ensure full carbon oxidation. The so-obtained mass retention vs. temperature plots are presented in Figure 4.

For pure sand, the small percentage of weight loss (0.1%) was associated with the impurities contained in the sample as the pure silica melting point was 1,610ºC [25]. No thermal degradation was, therefore, obtained for the pure sand sample within the selected operational temperature range (100ºC to 1,000ºC, 10 ºC/min). For both coloured sands, weight loss was associated with the degradation of the coating in the samples. As observed in Figure 4 and in both cases, carbon coating oxidation took place in a single step, although a difference in temperature appeared during this process occurs depending on the origin of carbon. The initial degradation temperature of both coloured samples is shown in the figure and was calculated as the temperature when 1.5% of weight was lost. This initial degradation temperature was read as the upper limit temperature that this material could work at without degradation. The CB-coated sample was stable for temperatures up to 645ºC, while the glucose-coated ones underwent oxidation at temperatures below 441ºC. Regarding the amount of carbon present in each coated sand, the CB presented a carbon content of 4.44%, while the carbon content for the glucose-coated sand was 5.99%.

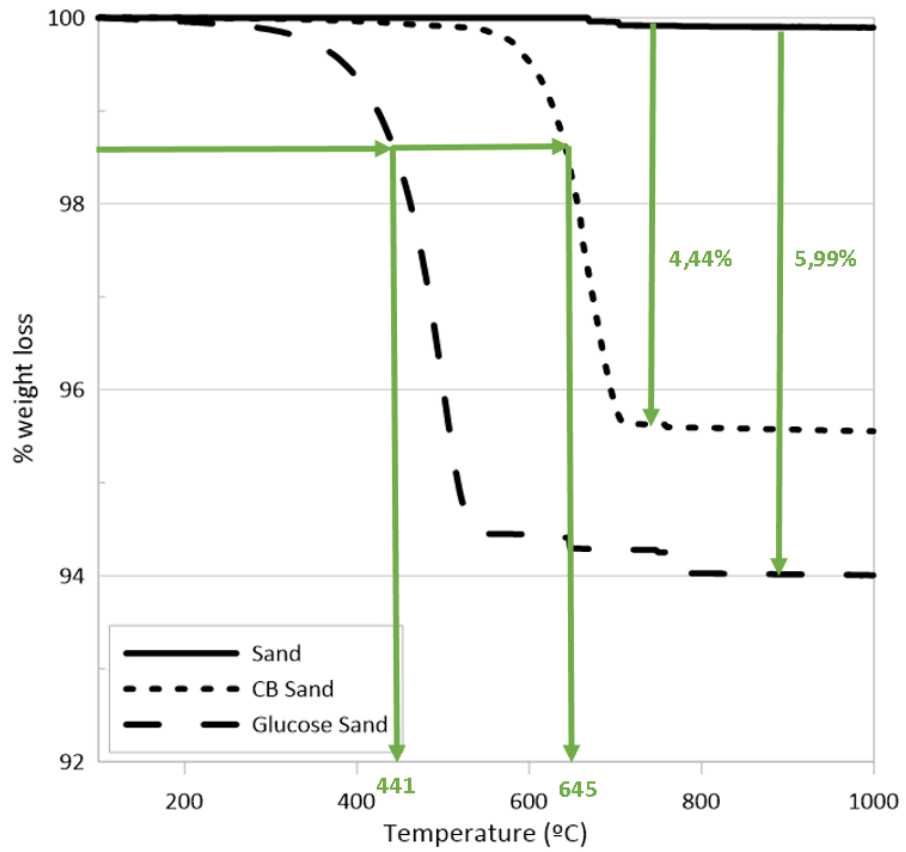

Figure 4. Weight loss *versus* temperature of the sand and carbon-coated sands.

3.2. Optical characterisation

The absorption spectrums of both coloured sand samples and the initial sand were evaluated to ensure that absorption improved. Figure 5 shows the absorption spectrums for the initial sand and those of the two coloured sand samples within the wavelength ranges from 400 – 800 nm and from 1,100 to 1,500 nm.

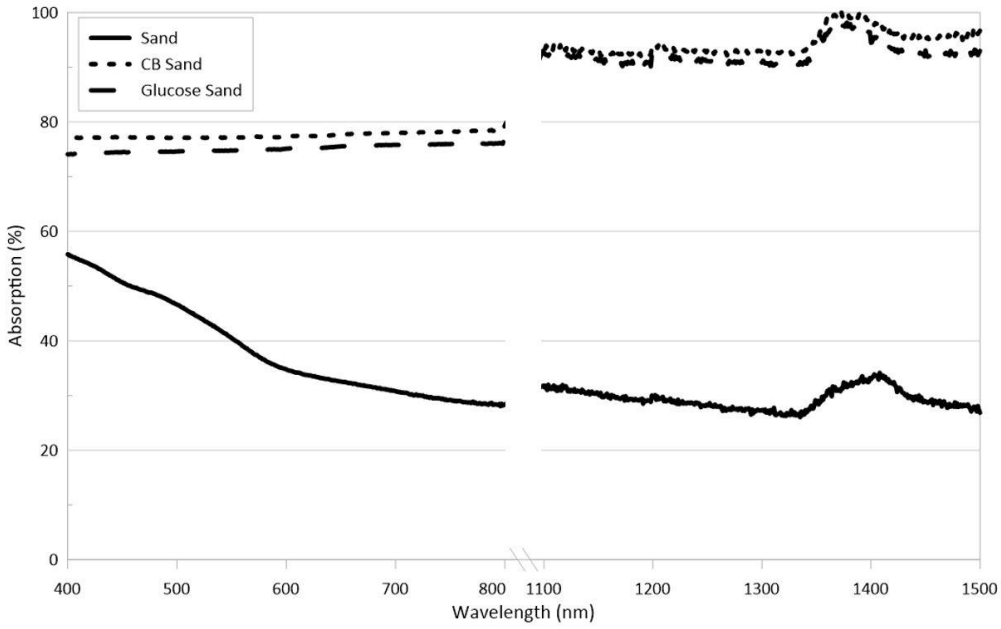

Figure 5. Sand absorption spectrums within the different measured wavelength ranges.

In both the carbon-coated samples, the absorption of the coloured sand was greater than that of the pure sand over the whole spectral range. The absorption of both coloured samples was more homogeneous for different wavelengths.

The averaged absorption increase of the coloured sands *versus* the pure sand was more marked for the CB sand within both wavelength ranges. For the 400-800 nm wavelength range, increments of 85% and 78% were obtained for the CB and glucose sand, respectively, and these values increased to 143% and 139% for the 1,100-1,500 nm range.

Given the possible application of sand samples in solar absorption systems, evaluating the sunlight-absorbed fraction (E) of samples was important. The sunlight absorbed fraction was considered when calculating absorption with the sand samples, following Equation 3:

$$E = \frac{\int_{\lambda min}^{\lambda max} I(\lambda) \cdot A(\lambda) d\lambda}{\int_{\lambda min}^{\lambda max} I(\lambda)\, d\lambda} \qquad \text{Eq. 3}$$

where I(λ) is the spectral distribution of the solar incident irradiance considered within the wavelength range (λ_{min}, λ_{max}) and A(λ) is the absorption spectra. Calculations were done according to Eq. 3, by using the CIE solar spectrum with an air mass m=1.5 for the solar incident irradiance [26] and considering the corresponding integration bounds for each wavelength range. The results are presented in Table 2, and show the corresponding amount of solar energy that the different samples within the various wavelength ranges were able to absorb.

Table 2. Solar energy absorbed by the three different sand samples within various wavelength ranges

Sample	E (%) 400 – 800 nm	E (%) 1,100 – 1,500nm	E(%) 400 – 800 + 1,100 – 1,500 nm
Sand	43	31	40
CB Sand	79	93	82
Glucose Sand	75	92	78

The listed values agree with the absorption spectrum values as the CB sand absorbed the most, followed by glucose sand, and finally by raw sand. As a relevant result, both coloured sands approximately doubled the absorbed fraction of the solar radiation compared to the initial raw sands within the studied wavelength range.

3.3. Thermo-physical characterisation

3.3.1. Specific heat capacity

Table 3 shows the specific heat capacity of the three different sand samples at various temperatures (300º, 400ºC and 500ºC).

As we can see, the specific heat capacity was temperature-dependent, and the results agree with those presented by Baumann and Zunft for the raw sand values of *Cp* [27].

When sand was coated, the obtained *Cp* values were slightly higher. This specific heat increase with the addition of coating on sand samples can be explained by the mixture rule that applies to this property and the higher specific heat of carbon *versus* sand at those temperatures [28]. However, these changes fell within the error of measurements, so only the global increase of Cp with the carbon coating can be concluded, and a more specific analysis of carbon coating in the initial sand was extracted from the TGA analysis.

Table 3. Specific heat capacity of three sand samples at three temperatures

	Cp (kJ/kg·K) at 300ºC	Cp (kJ/kg·K) at 400ºC	Cp (kJ/kg·K) at 500ºC
Sand	1±0.02	1.07±0.03	1.14±0.02
CB Sand	1.07±0.02	1.18±0.03	1.22±0.03
Glucose Sand	1.03±0.03	1.10±0.02	1.20±0.03

3.3.2. Thermal conductivity

The evolution of the thermal conductivity of the three samples with temperature (room temperature, 40°C, 80°C and 120°C) was measured and studied. Relative thermal conductivity was calculated by dividing coated sands and pure sand thermal conductivities (k_{cs} and k_s respectively). The evolution of thermal conductivity and its relative value for all the samples, together with the bar error corresponding to the five experimental measurements, are plotted in Figure 6.

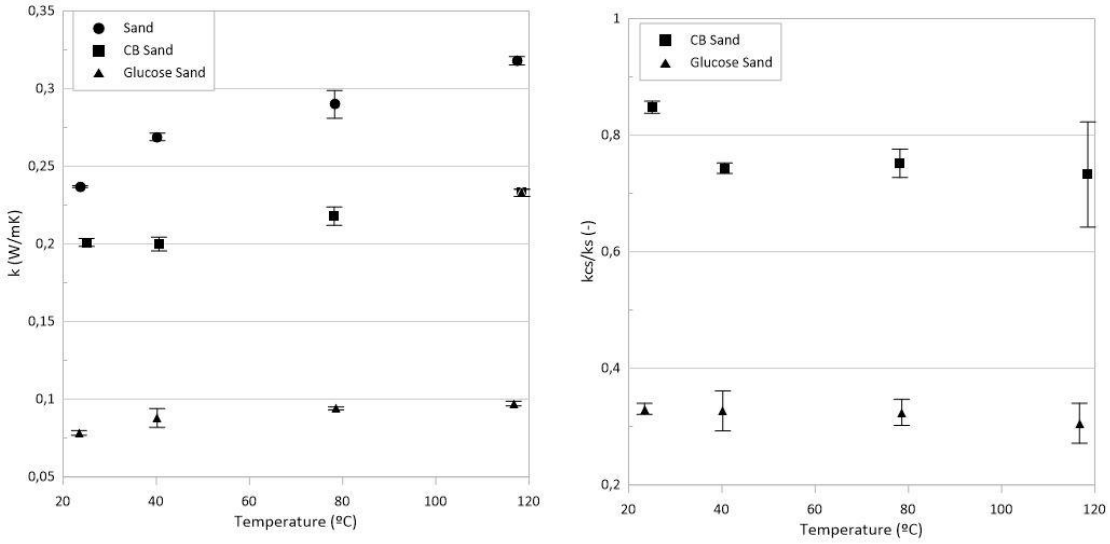

Figure 6. Evolution of thermal conductivity (left) and relative thermal conductivity with temperature (right)

The thermal conductivity results of the raw sand presented an increasing dependence with temperature and agree with the literature [26,29]. A weaker temperature dependence was shown for the coated sand samples.

For both coloured sands, thermal conductivity was lower than that of the raw sand, with average decreases of 55% and 45% for the CB sand and Glucose sand, respectively. These decreases can be explained by changes in porosity.

When comparing the thermal conductivity values and porosity values from Table 1 and Figure 6, thermal conductivity was seen to lower and be directly related with the porosity increments. This trend was also supported by research based on studying different sand types [30]. To estimate k, a semiempirical relationship was developed by Johansen in [31]:

$$k = \frac{0.135\rho_b + 64.7}{\rho_r - 0.947\rho_b} \qquad \text{Eq. 4}$$

where ρ_b is the bulk density of the sand sample (kg m^{-3}) and ρ_r is the real density of the sample (kg m^{-3}). The experimental and predicted thermal conductivity values, together with the corresponding relative errors, are presented in Table 4 for the three sand samples. A good agreement is shown, which therefore confirms the relationship between thermal conductivity reduction and porosity increments.

Table 4. Measured and predicted thermal conductivity values

	Measured Thermal conductivity (W/mK)	Predicted Thermal conductivity (W/mK)	Error (%)
Sand	0.213	0.256	18.3%
CB Sand	0.113	0.130	13.9%
Glucose Sand	0.082	0.086	4.9%

4. CONCLUSIONS

This work presents two methods to colour common silica sand from Silice Gllaranz (Spain) to be useful for direct absorption and TES materials in direct PSR.

The first was coloured by adding carbon black nanoparticles. The produced amount of coating was quantified as 4.44% wt. This sample presented lower density and higher porosity than the raw silica sand. The maximum working temperature for these samples was 645 ºC. Optical properties increased to 140% when absorption was measured. The Cp of the CB samples was higher than for the initial sand. Finally, thermal conductivity was slightly lower and this result agrees with the semiempirical relationship developed by Johansen.

The second colour process was that described when considering glucose being used as the main black colouring coating substance. The amount of produced coating was quantified as 6% wt. This sample presented higher porosity than the raw silica sand and CB samples. The maximum working temperature for these samples was 441ºC. Optical properties increased up to 140% when absorption was measured as in CB sample. The *Cp* of the glucose sand samples was higher than for the initial sand. Finally, thermal conductivity was slightly lower and this result also agrees with the semiempirical relationship developed by Johansen.

In short, the CB coating is more stable, present higher storage capacity (higher *Cp*), a higher maximum working temperature, and similar optical absorption and physical properties (density and porosity) to the glucose samples. Therefore, both coatings are good candidates in sand particles to be applied in direct particle solar receivers by bearing in mind that the maximum working temperature of carbon black coating is better than glucose.

ACKNOWLEDGEMENTS

This work has been partially funded by the Spanish government ENE2015-64117-C5-2-R (MINECO/FEDER). The authors would like to thank the Catalan Government for the quality accreditation given to their research group DIOPMA (2017 SGR118). LH and AGF acknowledges the financial support from the Generalitat Valenciana (Project: PROMETEU/2019/079) and from Pla de Promoció de la Investigació a l'UJI (Project: HTF-nano-PCM 16I359). The research was partially supported by EU COST Action CA15119 Nanouptake "Overcoming Barriers to Nanofluids Market Uptake". CB and MJ acknowledges EU COST Action CA15119 for their STMS grants.

REFERENCES

[1] C.K. Ho, B.D. Iverson, Review of high-temperature central receiver deigns for concentrating solar power, Renewable and Sustainable Energy Reviews 29, 835-846 (2014).

[2] C.K. Ho, Advances in central receivers for concentrating solar applications, Solar Energy. Article in Press.

[3] T. Tan, Y. Chen, Review of study on solid particle solar receivers, Renew. and Sust. Energy Reviews 14, 265-276 (2010).

[4] C.K. Ho. A review of high-temperature particle receivers for concentrating solar power. Appl Therm Eng 109, 958–69 (2016).

[5] Xu C, Wang Z, Li X, Sun F. Energy and exergy analysis of solar power tower plants. Appl Therm Eng 31, 3904–13 (2011).

[6] Ho CK, et al. Highlights of the high-temperature falling particle receiver project: 2012–2016. AIP Conf Proc 1850, 30027 (2017).

[7] Zhang H, Benoit H, Perez-Lopèz I, Flamant G, Tan T, Baeyens J. High-efficiency solar power towers using particle suspensions as heat carrier in the receiver and in the thermal energy storage, Renew Energy 111438–46 (2017).

[8] Wu W, Trebing D, Amsbeck L, Buck R, P-P. R, Prototype testing of a centrifugal particle receiver for high-temperature concentrating solar applications, J. Energy 137 (2015).

[9] Xiao G, Guo K, Ni M, Luo Z, Cen K. Optical and thermal performance of a high temperature spiral solar particle receiver, Sol. Energy 109, 200-213 (2014).

[10] Iniesta AC, Diago M, Delclos T, Falcoz Q, Shamim T, Calvet N. Gravity-fed combined solar receiver/storage system using sand particles as heat collector, heat transfer and thermal energy storage media. Energy Procedia 69, 802–11 (2015).

[11] Martin J, Vitko JJ. ASCUAS: A solar central receiver utilizing a solid thermal carrier. CA (USA): Livermore (1982).

[12] CK Ho , Highlights of the high-temperature falling particle receiver project: 2012–2016. AIP Conf Proc 1850, 30027 (2017).

[13] H. Zhang , H. Benoit, I. Perez-Lopez, G. Flamant, T. Tan, J. Baeyens, High-efficiency solar power towers using particle suspensions as heat carrier in the receiver and in the thermal energy storage, Renew Energy 111, 438–46 (2017).

[14] G. Xiao, K. Guo, M. Ni, Z. Luo, K. Cen, Optical and thermal performance of a high temperature spiral solar particle receiver, Sol. Energy, 109:200–13 (2014).

[15] Siegel NP, Ho CK, Khalsa SS, Kolb GJ, Development and Validation of a Prototype Solid Particle Receiver: On-Sun Testing and Model Validation, ASME J. Solar Energy Engineering 132 (2010).

[16] Falcone PK, Noring JE, Hruby JM, Assessment of a solid particle receiver for a high temperature solar central receiver system. Livermore, CA: Sandia National Laboratories (SAND85-8208) (1985).

[17] Ho CK, On-sun testing of an advanced falling particle receiver system. AIP Conf Proc 1734 (2016).

[18] I. Perez-Lopez, H. Benoit, D. Gauthier,m J.L. Sans, E. Guillot, G. Mazza, G. Flamant, On-sun operation of a 150kW pilot solar receiver using dense particle suspension as heat transfer fluid, Solar Energy 137, 463-476 (2016).

[19] M. Diago, A. Crespo-Iniesta, A. Soum-Glaude, N. Calvet, Characterization of desert sand to be used as a high-temperature thermal energy storage médium in particle solar receiver technology, Applied Energy 216, 402-413 (2018).

[20] H. Al-Ansary, A. El-Leathy, S. Jeter, E. Djajadiwinata, S. Alaqel, M. Golob et al., On-sun experiments on a particle heating receiver with red sand as the working medium, AIP Conference Proceedings 2033 (2018).

[21] New Mastersizer reduces sample volume for particle size analysis, Metal Powder Report, Volume 70, Issue 1, January– February 2015, Page 47.

[22] Diffuse Reflectance Accessory Manual. Varian CARY 500 Spectrophotometer.

[23] G. Ferrer et al., New proposed methodology for specific heat capacity determination of materials for thermal energy storage (TES) by DSC, Journal of Energy Storage 11 (2017) 1-6.

[24] Smits, K.M., Sakaki, T., Limsuwat, A., Illangasekare, T.H., "Thermal Conductivity of Sands under Varying Moisture and Porosity in Drainage-Wetting Cycles," Vadose Zone Journal, Volume 9, Number 1, pp. 172-180, (2010).

[25] Dr. Kamar Shah Ariffin (2004)9 What is Silica? EBS 425- Mineral Perindustrian.

[26] ASTM International, Standard Tables for Reference Solar Spectral Irradiances: Direct Normal and Hemispherical on 37º Tilted Surface, G173 (2012).

[27] T. Baumann, S. Zunft. Properties of granular materials as heat transfer and storage medium in CSP application. Sol. En. Mat. and Sol. Cells 143, 38-47 (2015).

[28] R.H. Perry, D.W. Green, J.O. Maloney. Perry's chemical engineers' handbook. McGraw-Hill (seventh edition) (2001).

[29] H. Kiyohashi, S. Sasaki, H. Masuda. Effective thermal conductivity of silica sand as filling material for crevices around radiactive-waste canisters. High Temperatures- High Pressures 35/36, 179-192 (2004).

[30] Smits, K.M., Sakaki, T., Limsuwat, A., Illangasekare, T.H., "Thermal Conductivity of Sands under Varying Moisture and Porosity in Drainage-Wetting Cycles," Vadose Zone Journal, Volume 9, Number 1, pp. 172-180, (2010).

[31] O. Johansen, Thermal conductivity of soils. Cold regions research and engineering laboratory (1977).